

## Observations of the Effects of Entrainment and Mixing on the Droplet Size Spectra in a Small Cumulus

JEFFREY L. STITH

*University of North Dakota, Grand Forks, North Dakota*

MARCIA K. POLITOVICH

*NOAA/ESG, Boulder, Colorado\**

(Manuscript received 13 June 1988, in final form 23 September 1988)

### ABSTRACT

Sulfur hexafluoride was released at the base of a small nonprecipitating, warm cumulus to study cloud mixing and entrainment processes. The tracer gas traveled to the top of the cloud where, during a 2.5 min period, it had mixed to produce a dilute mixture containing 30%, 19% and 51% of air from the original tracer region, an adjacent region of the same cloud, and the environment surrounding the cloud, respectively. The droplet size distributions measured at the top of the cloud represented a mixture of larger droplets that had been growing from the base and smaller, recently activated droplets. The observations suggest that the source region for the small droplets was near cloud top. The large droplet concentration was conserved during the mixing process. These observations are compared with predictions from some recent models for cloud entrainment and droplet evolution.

### 1. Introduction

Entrainment and mixing play an important role in the evolution of cloud droplet size distributions, but details of the processes involved are not fully understood and are the subject of some controversy (e.g., Reuter 1986; Telford 1987; Paluch and Knight 1987). A number of theoretical studies such as Squires (1958), Telford and Chai (1980) and Reuter and Yau (1987) have described the evolution of individual cloudy air parcels during entrainment and mixing. However, it has been difficult to determine the veracity of these model results because of the difficulty of tracking individual air parcels in the real atmosphere.

This paper follows the mixing history of a single release of tracer gas, sulfur hexafluoride ( $\text{SF}_6$ ), in a small nonprecipitating cumulus. The gas was released at the base of the cloud and was traced to near its top with an aircraft. This tracer method allowed us to track the evolution of the mixing and its effect on droplet growth in a Lagrangian reference frame. The results are compared with predictions from some current cloud entrainment and droplet evolution models.

---

\* Present affiliation: Research Applications Program, National Center for Atmospheric Research, Boulder, CO.

---

*Corresponding author address:* Dr. Jeffrey L. Stith, Department of Atmospheric Sciences, Box 8216, University Station, Grand Forks, ND 58202.

This study is part of a larger investigation into the transport, mixing, and activation of AgI seeding agents in convective clouds conducted by the North Dakota NOAA Federal/State Cooperative Program in Weather Modification (Reinking 1985). Earlier results from these investigations are reported in Stith et al. (1986) and Stith and Benner (1987).

### 2. Instrumentation and methodology

The University of North Dakota's Cessna Citation research aircraft was the primary source of cloud physics and  $\text{SF}_6$  measurements. Instrumentation used in these studies included a Particle Measuring Systems Forward Scattering Spectrometer Probe (FSSP) for measurement of cloud droplets, an inertial navigation and gust probe system for wind and turbulence measurements, a NCAR-type reverse-flow cloud temperature sensor, a Cambridge System design dewpoint hygrometer, pressure transducers for measurement of static and pitot pressures, and a fast response  $\text{SF}_6$  analyzer (Benner and Lamb 1985). Complete information on the instrumentation and calibration procedures are given in Stith et al. (1986) and Stith and Benner (1987). Data from the FSSP were recorded at 4 Hz and the other measurements were recorded at 24 Hz. The FSSP data were corrected for sizing and concentration errors incurred by optical coincidence and electronic dead time effects as described by Baumgardner et al. (1985).

A second aircraft, a Beechcraft Duke, was provided by Weather Modification, Inc. for release of SF<sub>6</sub>.

The cloud selected for this study was sampled on 10 June 1987 and was located approximately 40 km northwest of Dickinson, North Dakota. The cloud had a base temperature and pressure of 10.6°C and 788 mb. A single release of SF<sub>6</sub> was begun at 1731:33 MDT at an altitude of 1.94 km (all heights listed are MSL), about 160 m below the base. The release was started before the Duke passed beneath the cloud and continued until the Duke was past the edge of the cloud base. During the treatment the Citation sampled the cloud 540 m above the Duke in a parallel track, to document the initial cloud characteristics (pass 1). The treatment and initial sampling passes by the two aircraft were made in a direction roughly along the horizontal wind shear axis (80°–260°, true), from the downshear to the upshear side. The shear axis was estimated from an earlier sounding made by the Citation. The single tracer gas release lasted 50 s, covered a distance along the Duke flight track of 4 km, and used a total of 1.9 kg of SF<sub>6</sub>. The cloud was approximately 1.3 km wide at the Citation flight level during pass 1, so that the tracer release, which formed a single plume across the cloud base, extended well past the cloud.

Following the treatment pass the Citation ascended to cloud top and made repeated passes while awaiting the arrival of the tracer plume there. These cloud-top passes were made across the shear axis to optimize the chances of plume interception. A schematic of the flight patterns relative to the cloud is shown in Fig. 1a. During the cloud-top sampling period (1738–1747 MDT) the

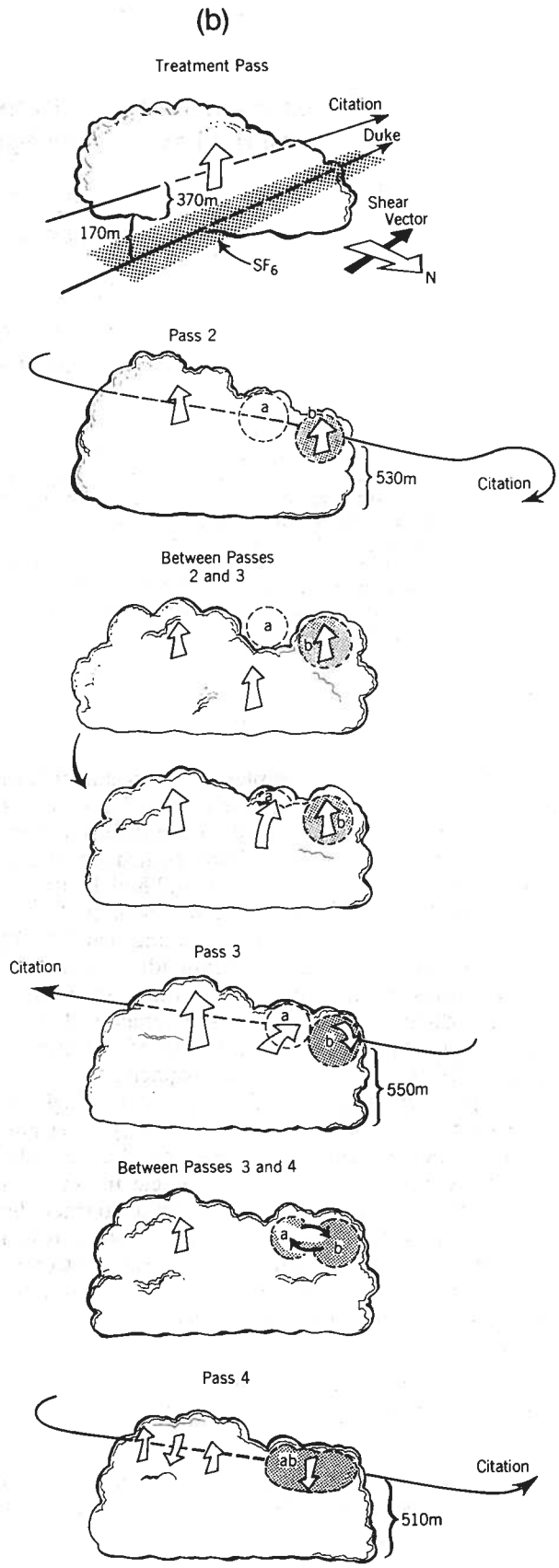
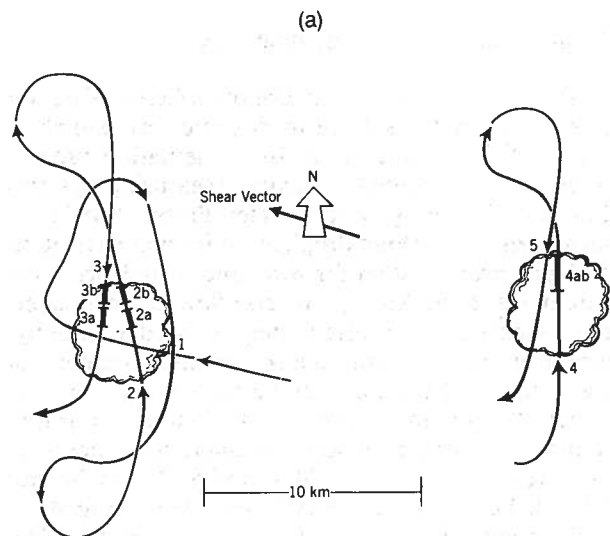


FIG. 1. Sampling of the 10 June cloud. (a) Plan view of Citation flight track, relative to the cloud motion based on the measured horizontal winds at the sampling altitude. Regions described in the text and approximate cloud outlines are indicated. (b) Schematic of processes described in the text. Regions a and b, flight tracks, air motions and SF<sub>6</sub> are indicated. The view is toward the southwest.

maximum altitude attained by the cloud turrets was estimated to be 100–300 m above the Citation. The temperatures at the flight levels near the cloud top were between 6 and 8°C.

Upon first interception of the SF<sub>6</sub> plume, a real time “pointer” system was initialized to assist in guiding the Citation back to the tracer location in later passes. The system displays heading, distance, elapsed time and altitude required to intercept a parcel of air assumed to be moving with the measured wind field. The addition of vertical advection information was new to the pointer system used in 1987. The ability to estimate the altitude of the tracer provided useful guidance in some instances, but was of limited value in regions where the clouds were experiencing rapid vertical accelerations (e.g., near the cloud tops). The horizontal portion of the pointer system is more reliable in locating cloudy plumes of SF<sub>6</sub>, particularly in smaller clouds such as this, but also eventually diverges from the region that has been tagged with SF<sub>6</sub>. These errors (due to accelerations of the region) were minimized by updating the pointer on each successive plume interception.

### 3. Observations

An environmental sounding taken within 40 km of the cloud (Fig. 2) revealed the environmental lapse rate to be almost dry adiabatic below the cloud and nearly moist adiabatic at cloud levels. This made the distribution of wet equivalent potential temperature almost constant with altitude at cloud heights, making a thermodynamic mixing analysis (see Paluch 1979) inapplicable in this case. The lack of sufficient instability at cloud levels limited the growth of this small cumulus.

The cloudy regions selected for analysis are indicated on the flight tracks and are shown schematically in Fig. 1b. A summary of the measurements obtained by the Citation is presented in Figs. 3 and 4 and Table 1.

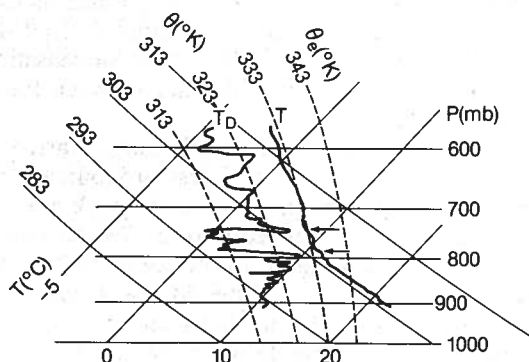


FIG. 2. The results of a partial sounding made by the Citation aircraft from 1726–1730 and 1820–1827 MDT. The sounding was made within 40 km of the study cloud. Arrows point to the cloud base and top.

During pass 1, a broad downdraft was observed downshear adjacent to an updraft of similar size and magnitude on the upshear side (Fig. 3, pass 1). In the updraft portion of the cloud the liquid water content and droplet concentration were positively correlated with the updraft magnitude.

The tracer was first detected during the cloud-top sampling (pass 2) in a small turret 0.4 km wide on the north side of the cloud (region 2b in Fig. 3) in an updraft of  $\sim 2 \text{ m s}^{-1}$ . An area of very low liquid water content, almost at rest in the vertical, was located just south of this region (region 2a, Fig. 3). The horizontal wind gust measurements indicated that both regions were moving north relative to the mean flow. The tracer region will be referred to as b, and the adjacent cloud extending 500 m to the south will be referred to as a.

During pass 3 the tracer was found at the same location at the northern edge of the cloud (region 3b, Fig. 3). Region 3b was about the same size as 2b, but had slightly higher tracer concentrations, which suggests that a more concentrated part of the SF<sub>6</sub> plume, located below the sampling altitude during the previous pass, had moved upward to this level during the 3 min between passes. Region 3b had nearly zero vertical velocity and a broad updraft had developed to its south.

A broader area of SF<sub>6</sub>, covering the entire cloud turret, was detected during pass 4 (Fig. 4), suggesting that tracer region 3b had mixed with nearby cloudy air, spread in extent through the turret, and became diluted during the 2.5 min between passes 3 and 4. Since the gust measurements during the previous pass suggested an overturning type of motion on the north side of the cloud (see Fig. 3 pass 3; 3a is pushed upward and north towards 3b), it is likely that the two cloudy regions 3a and 3b mixed to some degree between passes 3 and 4. This suggestion is consistent with the droplet measurements, as will be presented later. Since the tracer region during pass 4 appeared to contain air from both regions a and b, it will be referred to as region 4ab. Region 4ab and the cloud turret were descending at  $\sim 2 \text{ m s}^{-1}$ . Just over a minute later, during pass 5, the tracer was found with the last remains of the cloud turret in a slightly stronger downdraft (Fig. 4, pass 5). The virtual temperature in the cloud was within  $\pm 0.5^\circ\text{C}$  of the clear air value during each of the five passes, which indicates that the cloud remained close to buoyant equilibrium with the environment.

### 4. Interpretation: The evolution of the droplet size spectrum

We suggest the following sequence of events, which are pictured in Fig. 1b, to explain the observations. First, region a rose from cloud base, mixed with environmental air, came nearly to rest at the observation level of pass 2, and was penetrated during pass 2 just before the droplets it contained evaporated. Region b (the tagged region) had just arrived at the observation

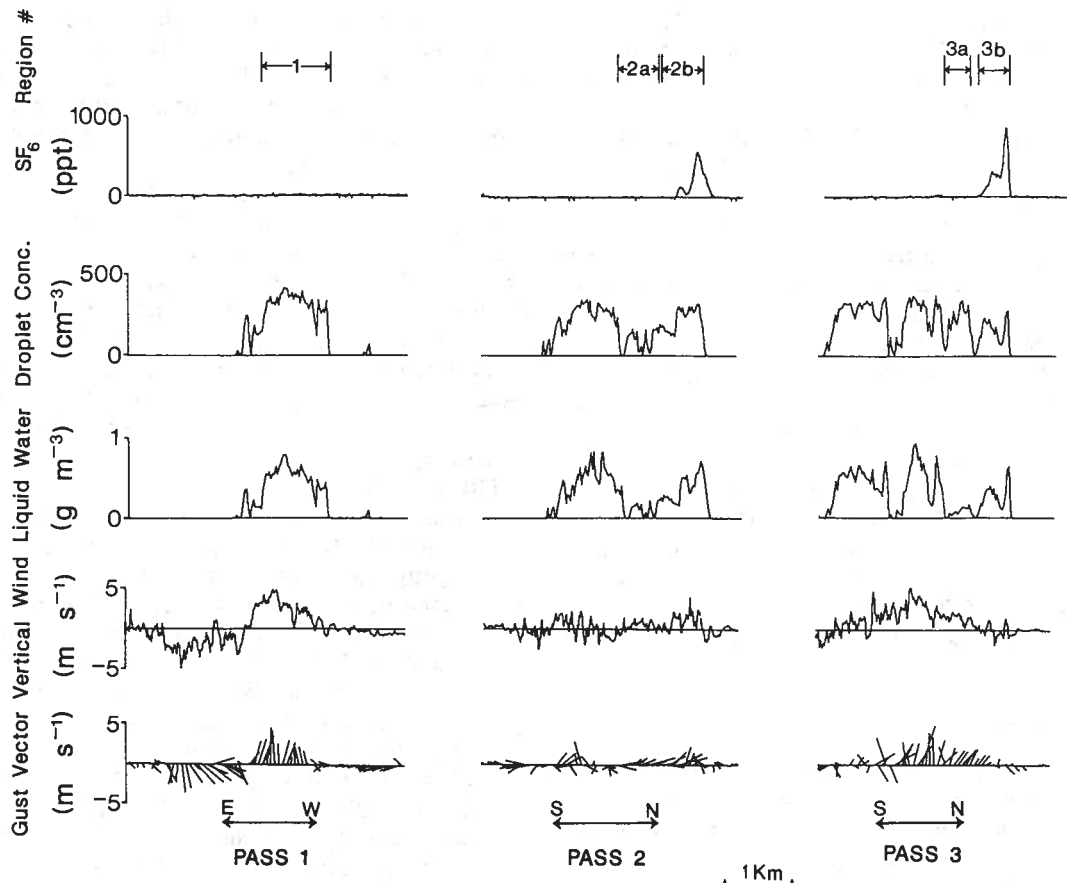


FIG. 3.  $\text{SF}_6$  concentration, droplet concentrations, FSSP liquid water content, vertical wind, and air motion in the vertical plane of the aircraft for passes 1, 2, and 3. Regions a and b (see text) are also indicated. Except for pass 1, data is displayed so that left-to-right corresponds to south-to-north in the cloud.

level during pass 2 and was still ascending slowly. Then, just prior to pass 3, the moistened but essentially droplet-free air in region a was pushed upward and northward by cloud rising beneath it and new droplets were activated. These small droplets were detected in region 3a. The tracer region encountered during pass 3, 3b, was essentially at rest when sampled. Between passes 3 and 4 regions 3a and 3b mixed to create the new region 4ab. The measurements supporting this hypothesis follow.

#### a. Rise of regions a and b from cloud base

The measurements from pass 1 indicate that the updraft region contained peak liquid water contents of 90% of the adiabatic value (Table 1); liquid water contents of well over 50% of adiabatic were sustained throughout most of the pass. In appendix A we show that adiabatic lifting from the base of the cloud would produce a droplet diameter of  $16.4 \mu\text{m}$ . The observed average droplet size distribution from pass 1 (see Fig. 5) was narrow with a strong peak in channels 4 and 5 of the FSSP ( $13.2\text{--}15.7 \mu\text{m}$ ); therefore, this peak was

most likely due to condensational growth. (The calculated value is that expected from adiabatic growth; this would likely be reduced slightly by the subadiabatic conditions in the upper cloud regions.) This peak persisted throughout the average and 4 Hz samples obtained from regions 2a, 2b and 3b (see Figs. 5, 6 and 7). However, the peak had broadened and included slightly larger sizes (including channel 6,  $15.7\text{--}19.4 \mu\text{m}$ ), which is expected from the further condensational growth in the  $160\text{--}180 \text{ m}$  difference between the observation levels.

During pass 2, region 2b, which had just arrived at the sampling level, exhibited a less pronounced peak than measured during pass 1 and the peak adiabatic liquid water fraction was reduced to 47%. Region 2a, the adjacent cloudy region to the south of 2b, had a maximum of only 18% of the adiabatic water. The spectral shape is similar to that from region 2b; the suggestion is that region 2a was more greatly affected by entrainment at the time of sampling.

Since region 2b contained  $\text{SF}_6$ , at least some of the air in this region must have come from the cloud base. This supports the observation of  $13\text{--}20 \mu\text{m}$  droplets in

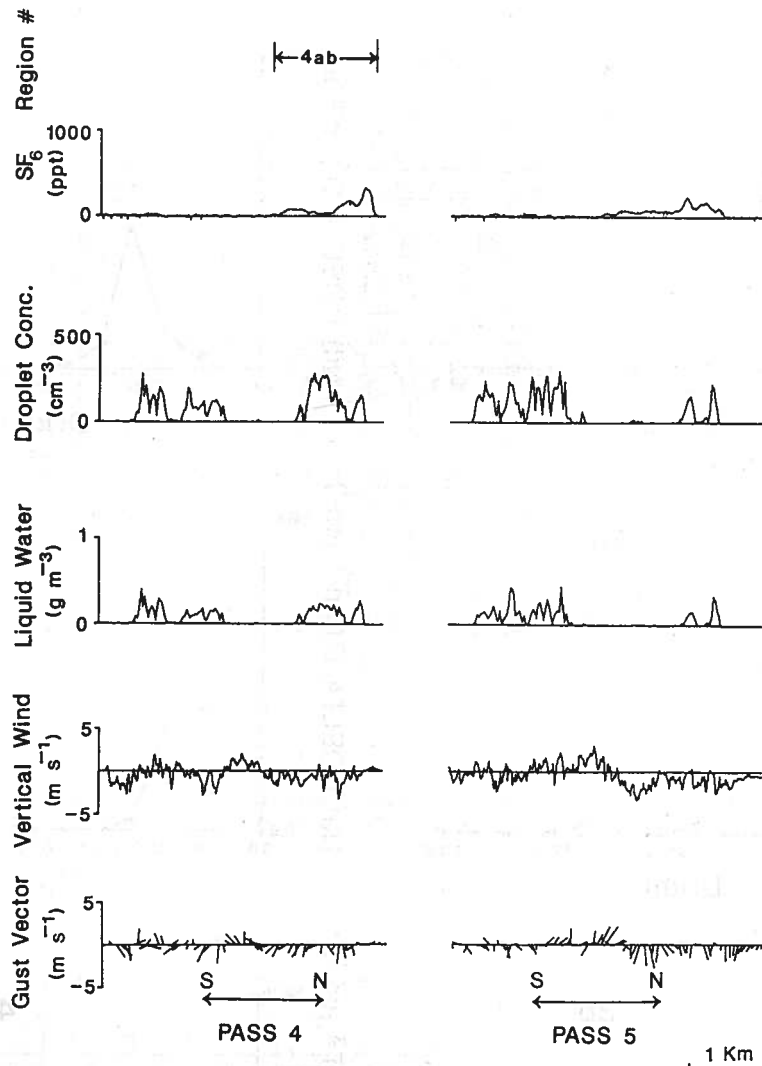


FIG. 4. As in Fig. 3, except for passes 4 and 5. Region 4ab is also indicated.

this region. The presence of a comparable but more dilute 13–20  $\mu\text{m}$  peak in the distribution from region 2a suggests a similar origin, but greater entrainment effects. The spectra from region 3b were similar to those

from 2b, as were the adiabatic liquid water fractions (41 and 47%, respectively, in Table 1).

#### b. Time for evaporation of droplets in region 3a

The region-averaged and 4 Hz FSSP data from region 3a (Figs. 5 and 7) indicate that the 13–20  $\mu\text{m}$  peak was virtually absent from the size distributions in this region. This suggests that further evaporation had taken place in region a between passes 2 and 3. A characteristic time for evaporation,  $T_{ev}$ , may be estimated following Baker et al. (1980) as

$$T_{ev} = \frac{10^{-6} \rho_w}{SD_a \rho_v} [(r + l)^2 - l^2] \quad (1)$$

where  $r$  is the droplet radius (in  $\mu\text{m}$ ),  $l$  is the length associated with the condensation coefficient ( $\sim 5 \mu\text{m}$ ),  $S$  is the supersaturation (in %),  $\rho_w$  and  $\rho_v$  are the den-

TABLE 1. Summary of cloud regions.

Region	Time (MDT)	Height above base (m)	Peak liquid water content ( $\text{g m}^{-3}$ )	Peak adiabatic fraction (%)
1 (updraft)	1732:39–1732:47	370	0.79	90
2a	1738:16–1738:21	540	0.28	18
2b	1738:22–1738:27	530	0.71	47
3b	1741:31–1741:35	550	0.63	41
3a	1741:37–1741:40	550	0.16	—
4ab	1743:53–1744:09	510	0.28	19

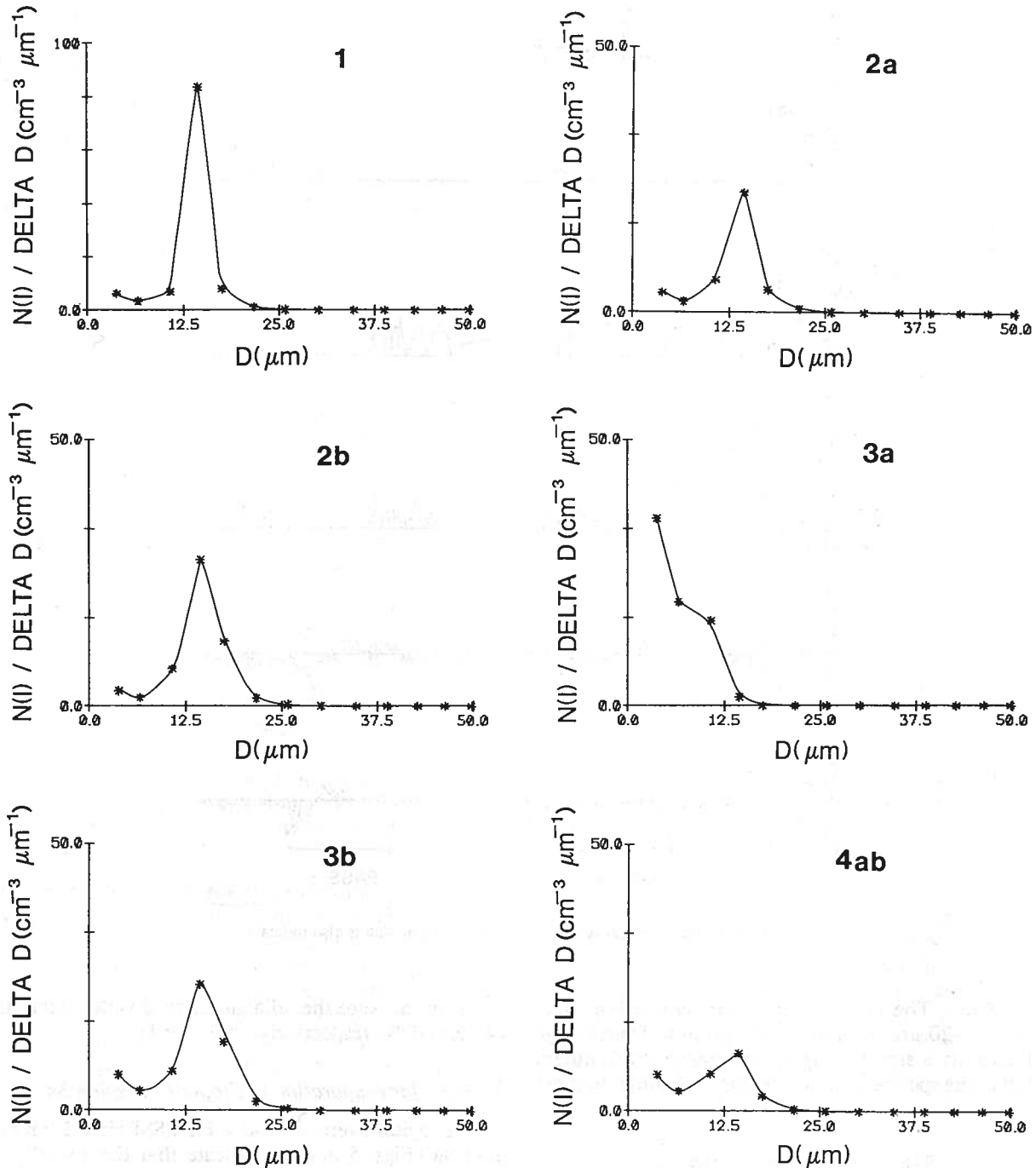


FIG. 5. Average droplet size distributions for each of the regions indicated in Figs. 3 and 4. The vertical axis represents the concentration per size interval. These data have been corrected using the techniques in Baumgardner et al. (1985).

sities of liquid water and saturated vapor ( $\rho_w \rho_v^{-1}$  is  $\sim 10^5$ ), and  $D_a$  is the molecular diffusion coefficient ( $\sim 0.25 \text{ cm}^2 \text{ s}^{-1}$ ). Even for a relatively slight subsaturation of  $S = -1\%$ , (1) predicts  $T_{ev}$  to be only  $\sim 1$  min for a  $16 \mu\text{m}$  droplet. Therefore, if sufficient dry air had been entrained into region 2a, there was enough time for even the larger droplets in this region to evap-

orate prior to the arrival of the broad updraft observed during pass 3.

c. Activation and growth of droplets in region 3a

The droplet spectra for region 3a were quite different from the other spectra (Figs. 5 and 7). Droplets in 3a

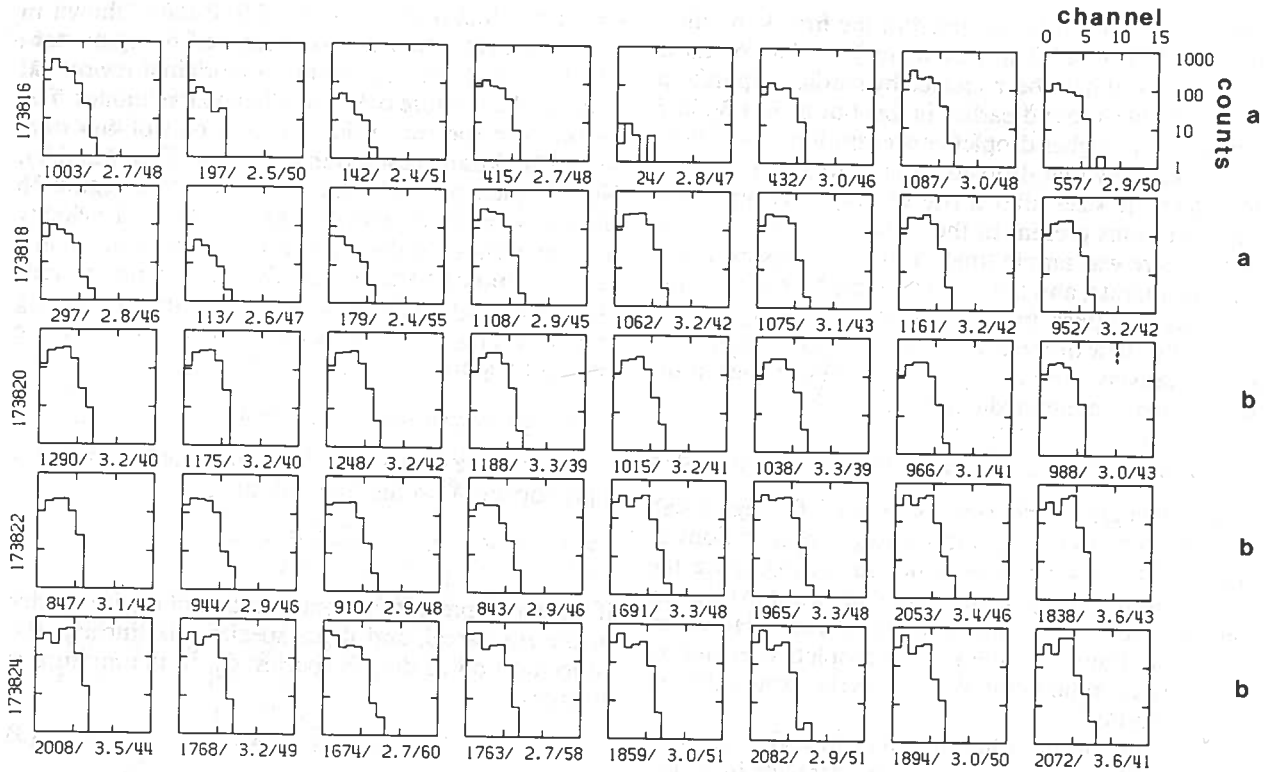


FIG. 6. FSSP counts versus channel number for 4 Hz samples obtained during pass 2. The numbers below each plot represent: total counts/mean channel number/dispersion (%). Each line of eight plots represents 2 s of data; the time of the first second is listed at the beginning of the line. Regions a and b are indicated.

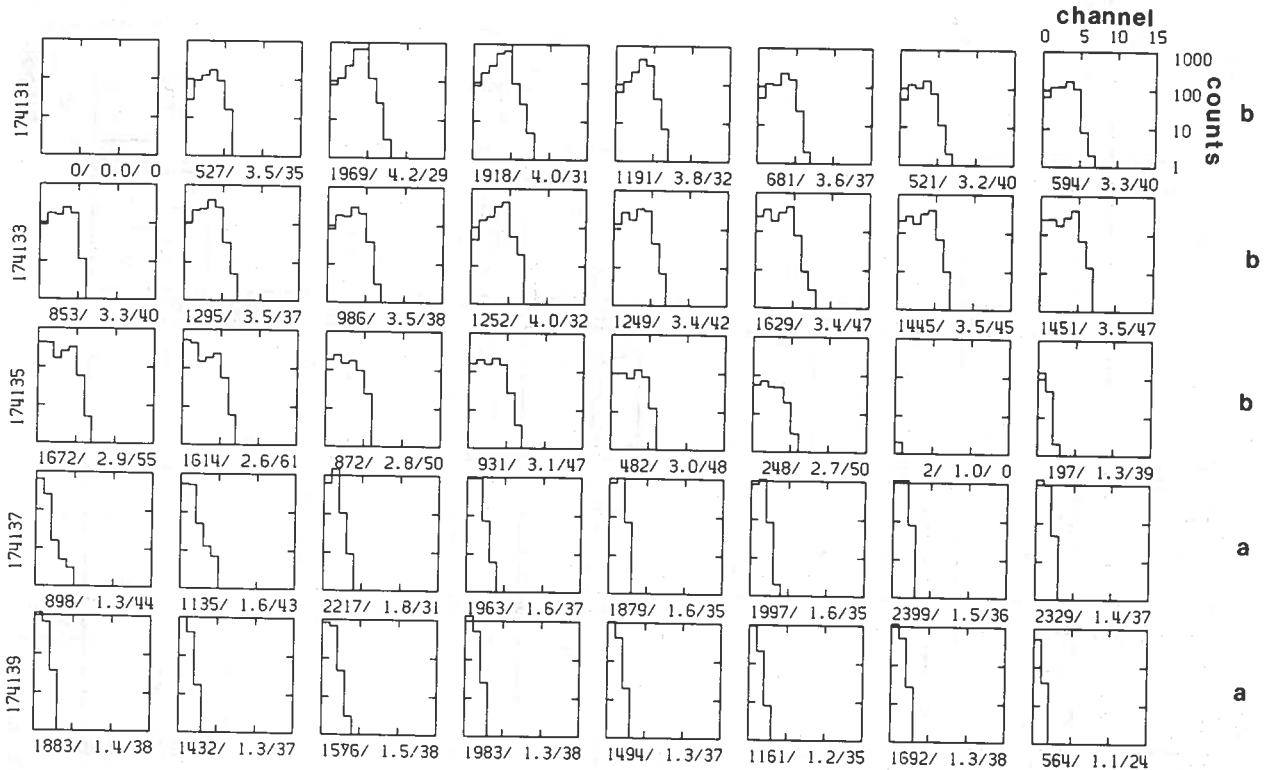


FIG. 7. As in Fig. 6, except for pass 3.

were small, with most detected in the first 3 channels of the FSSP ( $\leq 13.2 \mu\text{m}$  diameter). A few of these droplets could have been created by partial evaporation of the droplets found earlier in 2a, but region 3a had substantially higher droplet concentrations. In appendix A we show that droplets in saturated air can grow to detectable sizes after a rise of only  $\sim 10$  m, given the conditions present in the cloud. Between passes 2 and 3 there was ample time for the droplets in region 2a to evaporate, and then for the updraft observed during pass 3 to push region a upward, allowing the activation of new droplets there. This region would have been relatively close to saturation since just a few minutes earlier it contained cloudy air.

*d. Mixing of regions 3a and 3b to produce region 4ab*

The average droplet size distribution for region 4ab (Fig. 5) exhibits considerably lower concentrations of the 13–20  $\mu\text{m}$  sizes. This is not surprising, since the  $\text{SF}_6$  measurements indicate that considerable dilution had occurred, as was shown in Figs. 3 and 4. However, the concentrations of the smaller droplets were not reduced by a similar amount, as would be expected from such a dilution.

The small droplets found earlier in region 3a were the most likely source of the small droplets in region

4ab. Examination of the 4 Hz FSSP data (shown in Fig. 8) indicates that the southern half of region 4ab, which would have been nearer the original region 3a, contained a mixture of the small and large modes. The droplet size spectra in the northern part of 4ab were more like those measured in region 3b (Figs. 7 and 8). New droplets probably did not form within region 3b since it went from zero to negative vertical velocity between passes 3 and 4. The gust measurements shown in Fig. 3 indicate that region 3a was moving upward and toward region 3b, from south to north, suggesting an overturning type of motion which would mix these adjacent regions.

*e. Mixing proportions in region 4ab*

In a mixture of  $i$  parcels of air where each contributes a proportion  $X_i$  to the final mixture,

$$\sum_i X_i = 1. \tag{2}$$

If we let  $c_{ij}$  represent the concentration of the  $j$ th species in the  $i$ th parcel, and if the species mix linearly, the concentration of the  $j$ th species,  $C_j$ , in the mixture is given by

$$C_j = \sum_i c_{ij} X_i. \tag{3}$$

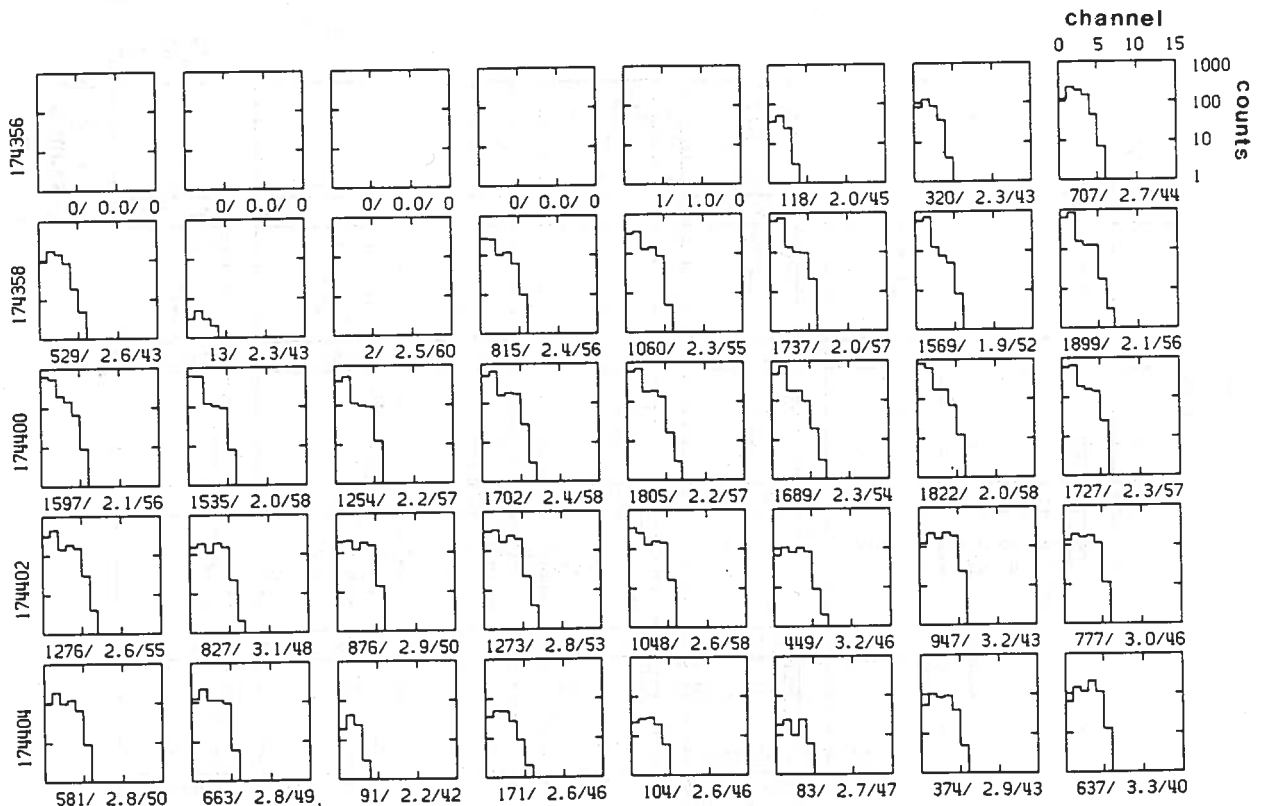


FIG. 8. As in Fig. 6, except for region 4ab.

A set of linear equations is formed by (2) and (3) which can be solved for  $X_i$ . Clearly, solving a particular system requires a sufficient number of tracer species,  $j$ , to provide a set of independent solutions.

One application of this approach is that once the proportions of air in a mixture are known, it is possible to assess the importance of nonlinear effects by comparing the mixing of the nonlinear species with that of a linear species such as  $\text{SF}_6$ . For example, cloud droplet concentrations are a nonlinear species because of the nonlinear effects caused by condensation or evaporation, sedimentation, and coalescence. For the present case the effects of sedimentation and coalescence are slight, owing to the small sizes of the droplets involved; but the effects of condensational growth or evaporation could be significant even for relatively short time scales and low super- or subsaturations. Mixing ratio, wet equivalent potential temperature (e.g., Paluch 1979) and  $\text{SF}_6$  are suitable linear mixing species. However, the first two require fast-response humidity measurements, for small clouds such as this one, which were not available. An additional advantage of using  $\text{SF}_6$  is that only one region involved in the mixture contained the tracer, which simplifies the solution of (2) and (3).

To apply this approach to the mixing process, which occurred between passes 3 and 4, note that region 4ab probably represented a mixture of air from regions 3a and 3b plus whatever cloud-free air had been entrained between passes 3 and 4. Regions 3a, 3b, and the cloud-free air will be associated with  $i = 1, 2$  and 3, respectively. For the  $\text{SF}_6$  ( $j = 1$ ) species, (3) may be rewritten as  $X_2 = C_1 c_{21}^{-1}$ , since the tracer was detected only in region 3b prior to mixing, i.e.,  $c_{11} = c_{31} = 0$ . Since region 3b was also the only one of the three regions to contain a significant number of large (diameter  $> 13.2 \mu\text{m}$ ) droplets ( $j = 2$ ),  $X_2 \sim C_2 c_{22}^{-1}$  if mixing (i.e., dilution) was linear. The large droplets which had been measured in region 2a had evaporated prior to pass 3 and thus were not found in region 3a (except for a few from the tail of the small droplet mode) as described in a previous section, so that  $c_{12} \ll c_{22}$ . The average concentrations (listed in Table 2) indicate that  $C_1 c_{21}^{-1} = 30.5\%$  and  $C_2 c_{22}^{-1} = 33.8\%$ , which is very close agreement given the accuracy of the measurements. Thus,

the concentration of large droplets in the mixture is that predicted by the observed dilution to within about 4%, indicating that the large droplets were nearly conserved during mixing. If the small droplets ( $j = 3$ ) were also conserved (i.e., mixed linearly), (3) gives

$$X_1 = \frac{C_3 - c_{23} X_2}{c_{13}} \quad (4)$$

Using  $X_2 = 30\%$  and (4), the final fraction of air from source region 3a in the mixture,  $X_1$ , is 19%. Since the concentration of small droplets,  $C_3$ , is that most likely to be affected by any evaporation which may have taken place, this value of  $X_1$  should be interpreted as a lower limit. Using the above values for  $X_1$  and  $X_2$  and (2), the resultant (maximum) fraction of environmental air,  $X_3$ , is 51%.

#### f. Turbulent mixing in region 4ab

The observation that the large droplets found in region 4ab had mixed in a linear fashion suggests that there was minimal droplet evaporation. This is unexpected since as much as half of the air in region 4ab may have come from drier cloud-free regions, and there was ample time for the droplets to evaporate between passes 3 and 4, as discussed earlier.

A possible resolution to the apparent conflict may be found in the Broadwell-Breidenthal (1982) model which describes mixing in a turbulent shear layer of thickness  $L$ . This has recently been applied to clouds by Baker et al. (1984). In this model, two mixing fluids intertwine with each other while maintaining their own properties and identities, in a marble cake type of pattern. Complete integration of one fluid into the other is not achieved until the scale of the turbulent mixing reaches the Kolmogorov microscale. The two fluids interact with one another along their interfacial surface, and this interfacial surface area per unit volume,  $A$ , grows according to

$$A \sim \frac{1}{L} \left(1 - \frac{t}{T_k}\right)^{-3/2}, \quad A < \frac{1}{\lambda_0} \quad (5)$$

where  $\lambda_0$  is the Kolmogorov length scale (typically a fraction of a centimeter in cumuli),  $t$  is the elapsed time since the onset of turbulent mixing, and  $T_k$  is the time required for complete homogenization of a region of size  $L$ . Here  $A$ , which is inversely proportional to the scale of the fluid distortions, grows slowly at first and then more rapidly as the size of the distortions approaches  $\lambda_0$ , as illustrated in Fig. 9.

If the mixing length scales at the time of sampling are smaller than resolved by the instruments (one 4 Hz sample covers approximately 20 m of cloud), the fluid properties, which in this case are the droplet or tracer concentrations, will appear diluted. During the early stages of mixing, when  $t \ll T_k$ , the amount of interfacial surface area between cloudy and subsatur-

TABLE 2. Average concentrations of  $\text{SF}_6$  and droplets before and after mixing. Refer to text for definition of terms.

Region	$i$	Large droplets ( $> 13.2 \mu\text{m}$ ) ( $\text{cm}^{-3}$ )			Small droplets ( $< 13.2 \mu\text{m}$ ) ( $\text{cm}^{-3}$ )		
		$\text{SF}_6$ (ppt)	$j = 1$	$j = 2$	$j = 3$		
3a	1	0		4.14		218	
3b	2	269		115		61.7	
environment	3	0		0		0	
4ab		82		38.9		60.9	

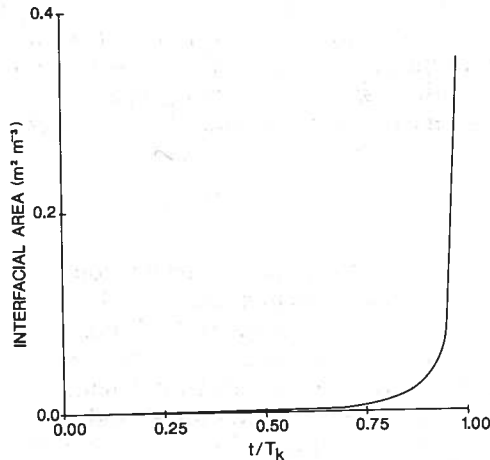


FIG. 9. Interfacial area per unit volume of air for a 1 km thick turbulent shear layer from (5) vs  $t/T_k$ .

ated regions is extremely small (Fig. 9). Consequently only a very few droplets are affected and little evaporation is observed, but the parcel appears diluted. Later, as the size of the fluid elements approaches the Kolmogorov scale, mixing becomes complete and the droplets evaporate. For a more detailed discussion of this process as it applies to clouds, see Baker et al. (1984).

The turbulent energy dissipation rate,  $\epsilon$ , was estimated (from airspeed fluctuations) to range between 10 and 100  $\text{cm}^2 \text{s}^{-3}$  during passes 3 and 4. With  $T_k \sim (L^2/\epsilon)^{1/3}$ , and  $L \sim 1$  km (the size of region 3a plus 3b),  $T_k \sim 460$  s for  $\epsilon \sim 100 \text{ cm}^2 \text{s}^{-3}$ . Therefore, during the 133 s between passes 3 and 4, with  $t/T_k \sim 0.29$  (or less), the amount of interfacial surface area predicted by the model is only a few  $\text{cm}^2$  per  $\text{m}^3$  (Fig. 9). The surface area is not predicted to reach appreciable proportions until at least 350 s after pass 3. Only partial evaporation was observed during pass 5 (Fig. 4), which began at 1746:20, some 280 s after pass 3.

##### 5. Comparison with previous studies of entrainment and droplet evolution

There is a large body of evidence (e.g., Paluch 1979; Boatman and Auer 1983; Jensen et al. 1985; and others) which suggests that cumuli entrain quantities of dry air at their tops, which subsequently mixes well into the cloud. Several mechanisms may be responsible for this further mixing. For example, the entrained region may become negatively buoyant and sink through the cloud as a penetrative downdraft, as first postulated by Squires (1958) and later modeled by Telford and Chai (1980) and others. Entrained regions may also be pushed aside by the growing cloud as suggested by Cooper and Rodi (1982). In the Fankhauser et al. (1982) conceptual model of the entrainment process, if insufficient negative buoyancy is created during en-

trainment, the mixed air remains near the entrainment level to form a layer of moistened air at that location. The 10 June observations are consistent with this description. Region 4ab was not favorable for development of substantial vertical instabilities due to low liquid water available for evaporative cooling, and the relatively moist environment as indicated by the sounding shown in Fig. 2. The maximum cooling achieved through total evaporation of the peak liquid water content found in region 3a amounts to only  $0.8^\circ\text{C}$ , after mixing with cloud-free air in a proportion of 49% to 51% as the results in the previous section suggest. Even with no further mixing this amount of negative buoyancy would allow descent only to cloud midlevels. Since most of region 3a had less liquid water than this, it is likely that at least a portion of the moist remains of region 4ab came to rest between the cloud midlevels and the cloud top.

The penetrative downdraft mechanism is probably not appropriate for smaller clouds such as this case. For a penetrative downdraft mechanism to be effective the subsaturated air parcels that form the downdraft must continue to mix with and evaporate nearby cloudy regions as the parcel descends. The 10 June case suggests that some of the subsaturated mixtures of cloud and environmental air may come to rest outside of the cloud. Consequently, they do not form penetrative downdrafts. A broad cloud-free downdraft was observed at cloud midlevels on the downshear side during pass 1 (Fig. 3). This subsaturated region was adjacent to, but outside of, the main cloud.

Mason and Jonas (1974) described a model of cumulus development in which successive thermals rise through and entrain material from the decaying residues of earlier thermals. This model and its later revisions (Jonas and Mason 1982) predict the activation of small droplets in older subsaturated cloudy regions by their interaction with new updrafts, as was likely in the 10 June cloud. But on 10 June the activation occurred near cloud top, whereas in the Mason and Jonas treatment activation takes place near cloud base as entrained subsaturated downdraft regions penetrate to lower levels of the cloud, where they interact with updrafts and renewed lifting activates new droplets.

The small droplets do not in this case appear to be produced in the manner described by Paluch and Knight (1984), who presented arguments to support significant new droplet production in cumuli at levels well above cloud base. The evidence for this was the correlation of observed peaks of small droplet concentrations with reduced concentrations of larger droplets within vigorous updrafts. This would have the effect of producing local increases in supersaturation which in turn allows activation of interstitial condensation nuclei. The small droplets in region 3a probably formed as the new updraft reactivated the condensation nuclei which remained after that region had previously evaporated, as was shown in a previous section. These

newly-formed droplets then were mixed with the larger droplets (in region 3b) which had cloud base origins.

## 6. Summary

Our results suggest a mechanism where cloudy regions mix with environmental air near the cloud top and evaporate completely, coming to rest subsaturated at a level not far from the cloud top. Rising air beneath this moistened air pushes it upward and new droplets are activated well above cloud base. This region subsequently mixes with an adjacent cloudy region, and the resultant mixture contains droplets with differing origins and histories, and thus different sizes. This mechanism is similar to that suggested by Politovich (1986) and Politovich and Cooper (1988) who showed that spectral broadening in cumuli could result from variations in growth histories between adjacent cloudy regions or from inhomogeneities in the cloud supersaturation. Austin et al. (1985) mention mixing of neighboring cloudy regions as a possible mechanism for production of bimodal size distributions but did not specifically investigate this possibility.

The tracer technique used in this analysis is a valuable tool for the study of cloud evolution, enabling a description of air parcel history in a Lagrangian framework. The expanding tracer boundaries and the tracer dilution can be measured, although definition of region boundaries in the adjacent non-tracer regions is admittedly more arbitrary. In the 10 June case, the release aircraft was able to pass under the cloud base region in approximately 10 s during treatment, so it is possible to determine the time from release with acceptable resolution.

We have demonstrated that, in this case, the cloud top was a source of newly activated droplets. This may provide an explanation for bimodal size distributions which are often found in similar clouds (e.g., Cooper and Rodi 1982; and Austin et al. 1985). The early mixing process for large droplets was found to be nearly linear, that is, significant evaporation did not occur and concentrations of these droplets were merely diluted as a result of the mixing event. These types of observations are needed to confirm theoretical studies and to further our understanding of the effect of entrainment and mixing in cumuli.

*Acknowledgments.* This work was supported by the North Dakota Atmospheric Resource Board through contract NDARB-UND-NOAA-87. MKP was sponsored by a National Research Council Associateship. Many thanks are due to R. Tilbury, E. Dondlinger, G. Herlache, M. Brown and D. Noah, who participated in the field studies, and to E. Robertson for typing the manuscript (University of North Dakota). R. Reinking (NOAA Weather Modification Program) and T. Uttal (NOAA Wave Propagation Laboratory) provided helpful comments on the manuscript.

## APPENDIX A

### Condensational Growth of Cloud Droplets

Following Politovich and Cooper (1988), a simplified form of the droplet growth equation may be written

$$r \frac{dr}{dt} = GS \quad (\text{A1})$$

where

$$G = \left[ \frac{\rho_w R_w T}{D_a e_s f_\beta} + \frac{L_v^2 \rho_w}{K R_w T^2 f_\alpha} \right]^{-1}$$

(Symbols are defined in appendix B). The supersaturation,  $S$ , may be approximated by its steady state value (as in Squires 1952, or Paluch and Knight 1984):

$$S \approx \frac{a_1 W}{a_2 I} \quad (\text{A2})$$

where

$$a_1 = \frac{L_v g}{R_w T^2 C_p} - \frac{g}{R_d T}$$

$$a_2 = \frac{4\pi}{\rho_a} \left[ \frac{P R_w}{R_d e_s} + \frac{L_v^2}{R_w C_p T^2} \right] \left[ \frac{T R_w}{f_\beta D_a e_s} + \frac{L_v^2}{f_\alpha K R_w T^2} \right]^{-1};$$

$W$  is the updraft speed, and  $I = \int r n(r) dr \sim N \bar{r}$ . This gives

$$r \frac{dr}{dt} = G \frac{a_1 W}{a_2 N \bar{r}} \quad (\text{A3})$$

We seek to estimate the size of a droplet that has grown by condensation after a total change in height  $\Delta Z$ . For this calculation we start with a uniform collection of newly activated droplets of size  $r_0 = 1 \mu\text{m}$ , and assume they encounter the same growth conditions. Thus they remain monodisperse and  $r = \bar{r}$ . Substituting  $dz = W dt$  and integrating (A3) gives

$$r^3 - r_0^3 = 3G \frac{a_1 \Delta Z}{a_2 N} \quad (\text{A4})$$

During pass 1, the cloud had near adiabatic liquid water content, an almost monodisperse size distribution, a droplet concentration of  $450 \text{ cm}^{-3}$ , and a broad, fairly smooth updraft (Figs. 3, 5 and Table 1). Consequently, the above assumptions should be reasonable for this case. Using the measurements obtained during pass 1 and (A4) gives  $r = 8.2 \mu\text{m}$ .

Using the conditions measured in region 3a, (A4) gives  $r = 2.8 \mu\text{m}$  (i.e.,  $5.6 \mu\text{m}$  in diameter) for  $\Delta Z = 10 \text{ m}$ . Droplets of this size should be detectable by the FSSP, which has a lower size cutoff of  $2.8 \mu\text{m}$  at the gain setting used.

Cloud base measurements were used to compute  $G$ ,  $a_1$ , and  $a_2$  for the pass 1 computation, and measurements from 2a were used for these constants in the 3a computation.

## APPENDIX B

## List of Symbols

$A$	Interfacial surface area per unit volume
$a_\alpha$	$K(2\pi RM_w T)^{1/2}/[\alpha p(C_v + R/2)]$ (see $f_\alpha$ , below)
$a_\beta$	$[2\pi/(R_w T)]^{1/2} D_a/\beta$ (see $f_\beta$ , below)
$c_{ij}$	concentration of $j$ th species in the $i$ th parcel
$C_j$	concentration of $j$ th species in mixture
$C_{p,v}$	specific heat of air at constant pressure, volume
$D_a$	diffusion coefficient for water vapor in air
$e_s$	saturation vapor pressure for water vapor
$f_\alpha$	$(r + \lambda)/[r + a_\alpha(r + \lambda)/r] =$ kinetic factor (cf. Fukuta and Walter 1970)
$f_\beta$	$(r + \lambda)/[r + a_\beta(r + \lambda)/r]$
$g$	acceleration of gravity
$K$	thermal conductivity of air
$L$	thickness of turbulent shear layer
$L_v$	latent heat of vaporization
$l$	the length associated with the condensation coefficient
$M_d$	molecular weight of dry air
$M_w$	molecular weight of water
$N$	total droplet concentration
$n(r)$	droplet size differential distribution
$P$	total air pressure
$r$	droplet radius
$\bar{r}$	mean droplet radius, $\int n(r)dr$
$R$	universal gas constant
$R_d$	gas constant for dry air [ $R/M_d$ ]
$R_w$	gas constant for water vapor [ $R/M_w$ ]
$S$	supersaturation $[(e - e_s)/e_s] \times 100$
$t$	time
$T$	temperature (K)
$T_{ev}$	Time scale for droplet evaporation
$T_k$	time to reach complete homogenization of a region of size $L$
$W$	vertical wind velocity
$X_i$	proportion of $i$ th parcel in a mixture
$\alpha$	accommodation coefficient (assumed 1)
$\beta$	condensation coefficient (assumed 0.04)
$\epsilon$	turbulent energy dissipation rate
$\lambda_0$	Kolmogorov length scale
$\lambda$	mean free path of an air molecule
$\rho_a$	density of air
$\rho_v$	density of water vapor
$\rho_w$	density of liquid water

## REFERENCES

- Austin, P. H., M. B. Baker, A. M. Blyth and J. B. Jensen, 1985: Small-scale variability in warm continental cumulus clouds. *J. Atmos. Sci.*, **42**, 1123-1136.
- Baker, M. B., R. G. Corbin and J. Latham, 1980: The influence of entrainment on the evolution of the cloud droplet spectra: I. A model of inhomogeneous mixing. *Quart. J. Roy. Meteor. Soc.*, **106**, 581-598.
- , R. E. Breidenthal, T. W. Choulaton and J. Latham, 1984: The effects of turbulent mixing in clouds. *J. Atmos. Sci.*, **41**, 299-304.
- Baumgardner, D., W. Strapp and J. Dye, 1985: Evaluation of the forward scattering spectrometer probe, Part II: Corrections for coincidence and dead-time losses. *J. Atmos. Oceanic Technol.*, **2**, 626-632.
- Benner, R. L., and B. Lamb, 1985: A fast response continuous analyzer for halogenated atmospheric tracers. *J. Atmos. Oceanic Technol.*, **2**, 582-589.
- Boatman, J. E., and A. H. Auer, 1983: The role of cloud top entrainment in cumulus clouds. *J. Atmos. Sci.*, **40**, 1517-1534.
- Broadwell, J. E., and R. E. Breidenthal, 1982: A simple model of mixing and chemical reaction in a turbulent shear layer. *J. Fluid Mech.*, **125**, 397-410.
- Cooper, W. A., and A. R. Rodi, 1982: Cloud droplet spectra in summertime cumulus clouds. Preprints *Conf. on Cloud Physics*, Chicago, Amer. Meteor. Soc., 147-150.
- Fankhauser, J. C., I. R. Paluch, W. A. Cooper, D. W. Breed and R. E. Rinehart, 1982: Air Motion and Thermodynamics. *Hailstorms of the Central High Plains*, vol. 1. *The National Hail Research Experiment*, C. A. Knight and P. Squires, Eds., Colorado Associated University Press, 95-149.
- Fukuta, N., and L. A. Walter, 1970: Kinematics of hydrometeor growth of a vapor-spherical model. *J. Atmos. Sci.*, **27**, 1160-1172.
- Jensen, J. B., P. H. Austin, M. B. Baker and A. M. Blyth, 1985: Turbulent mixing, spectral evolution and dynamics in a warm cumulus cloud. *J. Atmos. Sci.*, **42**, 173-192.
- Jonas, P. R., and B. J. Mason, 1982: Entrainment and the droplet spectrum in cumulus clouds. *Quart. J. Roy. Meteor. Soc.*, **108**, 857-869.
- Mason, B. J., and P. R. Jonas, 1974: The evolution of the droplet spectra and large droplets by condensation in cumulus clouds. *Quart. J. Roy. Meteor. Soc.*, **100**, 23-28.
- Paluch, I. R., 1979: The entrainment mechanism in Colorado cumuli. *J. Atmos. Sci.*, **41**, 1801-1805.
- , and C. A. Knight, 1984: Mixing and the evolution of cloud droplet size spectra in a vigorous continental cumulus. *J. Atmos. Sci.*, **41**, 1801-1815.
- , and —, 1987: Reply. *J. Atmos. Sci.*, **44**, 2355-2356.
- Politovich, M. K., 1986: A study of the broadening of droplet size distributions in cumuli. Ph.D. dissertation, College of Engineering, University of Wyoming, 198 pp.
- , and W. A. Cooper, 1988: Variability of the supersaturation in cumulus clouds. *J. Atmos. Sci.*, **45**, 1651-1664.
- Reinking, R. F., 1985: An overview of the NOAA Federal-State Cooperative Program in weather modification research, *Fourth WMO Sci. Conf. on Weather Modification*, WMO/IAMAD Symposium, Honolulu, WMO/TD-NO 33, Geneva, II, 643-648.
- Reuter, G. W., 1986: A historical review of cumulus entrainment studies. *Bull. Amer. Meteor. Soc.*, **67**, 151-154.
- , and M. K. Yau, 1987: Mixing mechanisms in cumulus congestus clouds. Part II: Numerical Simulations. *J. Atmos. Sci.*, **44**, 798-827.
- Squires, P., 1958: Penetrative downdrafts in cumuli. *Tellus*, **10**, 381-389.
- Stith, J. L., and R. L. Benner, 1987: Applications of fast response continuous SF<sub>6</sub> analyzers to in situ cloud studies. *J. Atmos. Oceanic Technol.*, **4**, 599-619.
- , D. A. Griffith, R. L. Rose, J. A. Flueck, J. R. Miller, Jr. and P. L. Smith, 1986: Aircraft observations of transport and diffusion in cumulus clouds. *J. Climate Appl. Meteor.*, **25**, 1959-1970.
- Telford, J. W., 1987: Comments on "Does mixing promote cloud droplet growth?" *J. Atmos. Sci.*, **44**, 2352-2354.
- , and S. K. Chai, 1980: A new aspect of condensation theory. *Pure Appl. Geophys.*, **118**, 720-742.